

A Closed-Loop Multi-Agent Framework for Aerodynamics-Aware Automotive Styling Design

Xinyu Jin¹, Shengmao Yan¹, Qingtao Wang¹, Shisong Deng¹,
Yanzhen Jiang¹, Shuangyao Zhao^{1,2*}

¹School of Management, Hefei University of Technology, Hefei, China

²Key Laboratory of Process Optimization and Intelligent Decision Making, Hefei, China

Abstract

The core challenge in automotive exterior design is balancing subjective aesthetics with objective aerodynamic performance while dramatically accelerating the development cycle. To address this, we propose a novel, LLM-driven multi-agent framework that automates the end-to-end workflow from ambiguous requirements to 3D concept model performance validation. The workflow is structured in two stages: conceptual generation and performance validation. In the first stage, agents collaborate to interpret fuzzy design requirements, generate concept sketches, and produce photorealistic renderings using diffusion models. In the second stage, the renderings are converted to 3D point clouds, where a Drag Prediction Agent, built upon a lightweight surrogate model, provides near-instantaneous predictions of the drag coefficient and pressure fields, replacing time-consuming CFD simulations. The primary contribution of this work is the seamless integration of creative generation with a rapid engineering validation loop within a unified, automated system, which provides a new paradigm for efficiently balancing creative exploration with engineering constraints in the earliest stages of design.

1 Introduction

Automotive exterior design remains a complex negotiation between stylistic appeal and aerodynamic efficiency. Visually striking forms often compromise drag and stability, while purely physics-driven shapes may not meet market expectations. As shown in Figure 1 conventional workflows attempt to reconcile this tension through sequential phases: requirements analyses, designers sketch concepts, digital modellers create three-dimensional representations, and engineers conduct computational fluid dynamics (CFD) simulations and wind-tunnel tests. Because CFD runs can take hours or days, rigorous aerodynamic validation typically occurs late in the process, forcing costly redesigns and compromises when poor performance is discovered.

Recent advances in generative models (Ho, Jain, and Abbeel 2020) and Large Language Model (LLM) driven multi-agent systems (Wu et al. 2023) offer an opportunity to rethink this pipeline. Diffusion models yield photorealistic

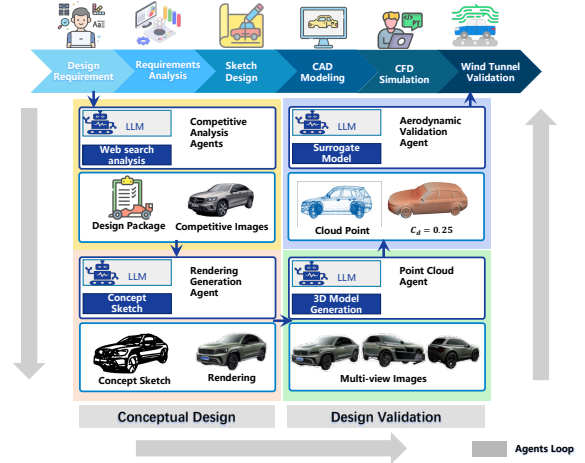


Figure 1: Illustration of the proposed multi-agent framework. Our framework contributes to the early design exploration and rapid aerodynamic validation compared to traditional methods.

tic images conditioned on text or sketches, and LLM frameworks such as AutoGen enable specialized agents to collaborate on complex tasks. However, existing design pipelines either apply generative models in isolation, leaving a gap to engineering validation, or rely on single-agent systems whose scalability and robustness remain unclear. In contrast, our work introduces a *closed-loop* design-validation workflow that seamlessly couples creative exploration with rapid aerodynamic assessment. The key insight is to embed generative and surrogate models within an LLM-orchestrated multi-agent system, so that high-level design prompts automatically trigger concept generation, 3D reconstruction and near-real-time aerodynamic prediction, which can dramatically accelerate the design process.

Compared with recent work (Elrefaie et al. 2025), our framework introduces several key improvements and innovations. First, during the CAD modeling stage, we reconstruct point cloud models from multi-view images instead of retrieving matches from existing models. This approach offers greater flexibility and practical value in real-world design workflows. Second, we adopt a fixed yet extensible

*Corresponding author.

agent-based workflow rather than relying on a LLM to coordinate all agent operations. This modular design enhances system stability, interpretability, and scalability, making it well-suited for evolving design pipelines. In addition, we incorporate a physics-attentive surrogate model capable of simultaneously predicting key aerodynamic indicators, including drag, pressure distribution, and velocity fields. The proposed model demonstrates superior performance on standard automotive aerodynamic benchmarks.

This paper introduces a novel framework that significantly advances the automotive design process by integrating LLM within a multi-agent collaborative system. Our contributions can be summarized as follows:

- The seamless and continuous integration of "Aesthetic-to-Performance": Our system establishes direct bridge between subjective aesthetic attributes and quantifiable aerodynamic metrics. The multi-agent system can inherently incorporate various engineering constraints from the initial conceptualization, ensuring that aesthetically pleasing designs are also technically viable and performant.
- Specialized Agent Autonomy and Collaboration: Distinct agents (e.g., the "Competitive Analysis Agents") are empowered with specific domain findings and can autonomously execute tasks.
- Facilitate rapid prototyping and exploration: The generative capabilities of the multi-agent system, combined with its understanding of design principles and constraints, enable the rapid generation of diverse design variations that adhere to initial aesthetic goals while considering performance implications from the outset.

2 Related Work

2.1 Generative Models in Concept Design

In recent years, Deep Generative Models have undergone explosive development. Early research methods typically utilized VAEs (Kingma and Welling 2014) and GANs (Goodfellow et al. 2014; Karras, Laine, and Aila 2019) to generate novel images, while the recent wave of technologies represented by Diffusion Models (Ho, Jain, and Abbeel 2020) marks a paradigm shift. These new models have achieved unprecedented levels of quality, diversity, and controllability in generated content, advancing AI image generation from a phase of "random creation" to a practical stage of being "controllable, usable, and customizable" (Labs et al. 2025). The latest advancements, exemplified by models like Stable Diffusion (Rombach et al. 2021) and DALL-E (Ramesh et al. 2021), fully demonstrate the immense potential of this field. Not only can they create detail-rich images based on complex textual instructions (Text-to-Image), but they have also fostered a vast community ecosystem. For instance, plugins like ControlNet (Zhang, Rao, and Agrawala 2023) allow users to exert precise geometric control over the generation process through inputs such as sketches (Sketch-to-Image) or poses. In creative fields such as automotive design, researchers have leveraged these advanced models to rapidly generate a vast number of conceptual visuals, sig-

nificantly accelerating the creative ideation phase and effectively exploring the aesthetic solution space (Burnap, Hauser, and Timoshenko 2023; Morita et al. 2024). However, a notable limitation of such work is its isolated focus on visual generation. The outputs are typically static images, lacking a direct pathway to engineering analysis, which leaves the critical loop between aesthetics and performance disconnected.

2.2 Surrogate Models for Aerodynamic Prediction

To address the issues of traditional CFD methods being computationally expensive, time-consuming, and difficult to integrate into generative design processes, researchers are utilizing data-driven surrogate models to significantly increase simulation speed while maintaining high accuracy (Qi et al. 2017). Early surrogate models predominantly relied on parameterized representations for performance prediction. For instance, vehicle profiles were characterized using discrete sets of control-point coordinates, and computational models were subsequently trained to estimate corresponding drag coefficients (Gunpinar et al. 2019; Rosset et al. 2023). Nevertheless, this method tends to oversimplify the geometric complexity of the automobile's shape, thereby limiting its applicability in practical design environments. To enhance shape feature extraction and representation, subsequent iterations of surrogate models have investigated learning-based methods utilizing two-dimensional or three-dimensional representations (Arechiga et al. 2023). For example, three-dimensional automotive geometries are projected onto two-dimensional planes from various viewpoints, and implicit representations are learned using sophisticated neural network architectures, such as irregular convolutional neural networks or graph neural networks, to predict the drag coefficient (Song et al. 2023; Jacob et al. 2022) and neural network-based surrogates can be deployed at industrial scale (Alkin et al. 2025). Additionally, generative models have been employed to reconstruct shapes from latent representations and predict pressure fields and drag coefficients, facilitating rapid and precise performance assessments (SAHA et al. 2021; He, Luo, and Wang 2025).

2.3 LLM-Powered Multi-Agent Systems

Traditional design and simulation workflows often rely on rigid pipelines, siloed expert knowledge, and manual iterations, which severely limit scalability, adaptability, and cross-domain collaboration. Multi-Agent Systems (MAS) have emerged as a powerful paradigm for solving complex, distributed problems by enabling autonomous agents to collaborate, plan, and execute tasks (Chen et al. 2024). With the rapid development of LLMs, the design and orchestration of such systems have entered a new era. LLMs now act as versatile cognitive engines that empower agents with advanced capabilities in reasoning (Yao et al. 2023), planning (Shinn et al. 2023), tool use (Schick et al. 2023), and inter-agent communication (Liu et al. 2025; Lu et al. 2024). This shift has led to the emergence of numerous LLM-centric multi-agent frameworks, such as AutoGen (Wu et al. 2023),

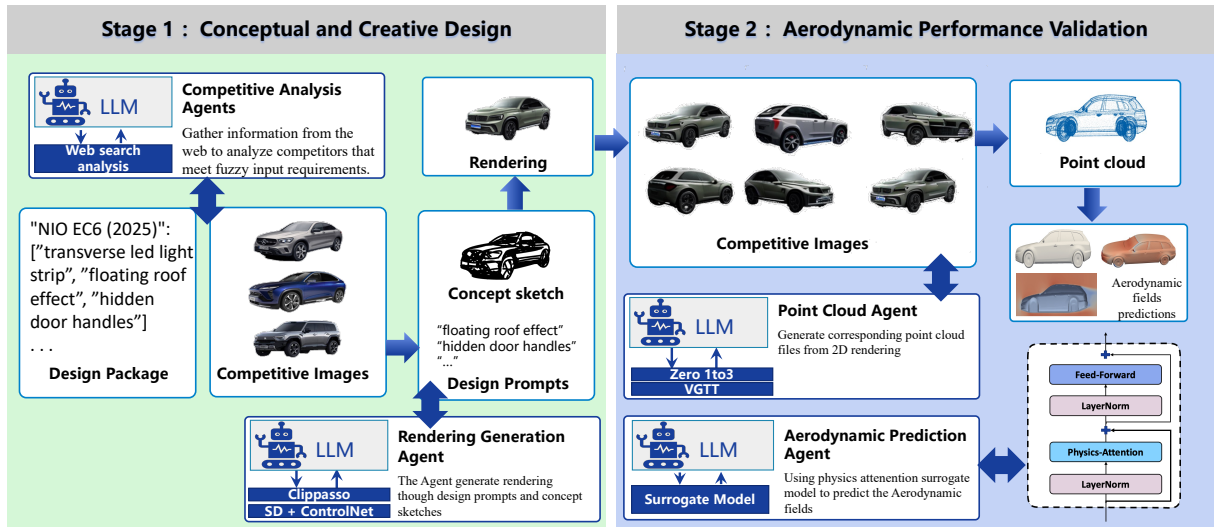


Figure 2: Overview of the proposed two-stage multi-agent framework. The first stage focuses on conceptual design, where user requirements are translated into visual concepts. The second stage emphasizes aerodynamic performance validation, utilizing surrogate models for rapid feedback.

LangChain (Zhang et al. 2025), and ChatDev (Qian et al. 2023), which enable the dynamic coordination of agents specialized in different tasks across domains including document processing (Ye et al. 2023), software development, and robotic control. In the design and simulation domain, recent efforts have explored the use of LLM-powered agents to automate multidisciplinary workflows. For instance, using agent assistants for semiconductor manufacturing (Chen et al. 2025). A recent work proposed a pioneering multi-agent system for joint aesthetic and aerodynamic car design (Elrefaie et al. 2025).

3 Method

3.1 Overview: A Two-stage Approach

In this section, we present a two-stage design process, illustrated in Figure 2, built upon the AutoGen multi-agent framework, deconstructs the complex automotive design process into a logical, automated workflow. Stage one focuses on conceptual design, translating ambiguous user requirements into photorealistic renderings. Stage two is dedicated to rapid aerodynamic performance validation, transforming the rendering into an analyzable 3D model and using a lightweight surrogate model for near-instantaneous feedback. This creates a rapid, closed loop from creative concept to engineering validation.

3.2 Conceptual and Creative Design

The primary objective of this stage is to rapidly transform a designer’s abstract ideas into a diverse portfolio of high-fidelity, visually compelling concept designs. Traditionally, this process has depended heavily on manual efforts—designers would conduct extensive market research, draft preliminary sketches, and carry out detailed rendering, often requiring significant time and domain expertise.

In contrast, our proposed multi-agent framework fully automates this pipeline by decomposing the task and distributing it among specialized agents. Specifically, the Competitive Analysis Agents performs real-time market analysis to identify trends, benchmarks, and differentiators, while the Rendering Generation Agent translates design intentions into high-quality visual outputs.

Competitive Analysis Agents The Competitive Analysis Agents comprises a team of collaborative sub-agents that translate high-level design requirements (e.g., a sporty SUV for the Chinese market with an aggressive appearance) into actionable market insights. Instead of performing a superficial, one-time search, it follows the “search-reflect” iterative loop shown in the Figure 3, continuously optimizing queries based on ongoing analysis and deepening its dive into market information until a comprehensive insight is formed.

Generated Exploration Plan Example

requirement: “A sporty SUV in the 300-500k RMB price range with an aggressive exterior, powerful performance, and a tech-focused interior”,
queries: [“300-500k RMB sporty SUV recommendations 2024”, “Top-rated SUVs with aggressive exteriors 300-500k RMB”, “Powerful performance SUV model comparison 300-500k RMB”, “Latest reviews of SUVs with high-tech interiors”]

Upon completion of the loop, the agents synthesize their research into a structured design package, which systematically maps key competitors to the high-level design prompts derived from their distinctive features. This transforms raw market data into an organized and actionable format. The resulting output—comprising semantically rich design prompts and a curated image library for visual refer-

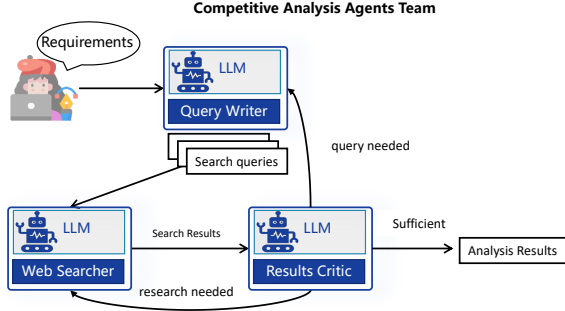


Figure 3: search-reflect iterative loop of the Competitive Analysis Agent.

ence—forms a robust, data-driven foundation for the subsequent creative sketching phase. This ensures that the final design is both aligned with designer intent and attuned to prevailing market trends.

Design Package

"NIO EC6 (2025)": ["transverse led light strip", "floating roof effect", "hidden door handles"]
 "Mercedes-Benz GLC Coupe (2025)": ["luminous grille", "fastback silhouette"]
 "Mengshi M817 (2025)": ["luminous grille", "hardcore off-road styling"] ...

Rendering Generation Agent After the "design package" is produced, the workflow is handed over to the Rendering Generation Agent. This agent's task is to creatively visualize the design concepts by generating high-fidelity renderings based on the insights provided by the Competitive Analysis Agents.

The first step for this agent is to generate a diverse set of concept sketches. It uses the Clipasso model to process the image library of competitor vehicles obtained in the previous step, generating a series of concept sketches in various artistic stroke styles, as shown in Figure 4, to provide designers with rich, unconventional early-stage creative inspiration.

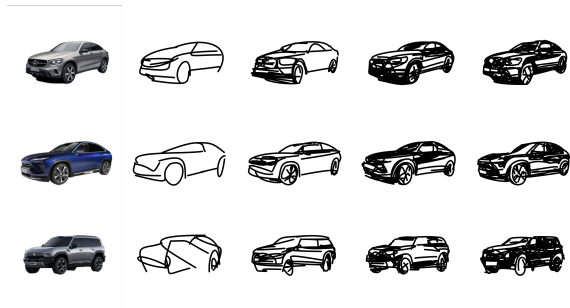


Figure 4: Concept sketches generated from a source image (left) via the Clipasso model, using 10, 25, 50, and 100 strokes to control the level of abstraction.

Subsequently, the agent converts these sketches into pho-

torealistic renderings. This process synergistically employs ControlNet and Stable Diffusion models to achieve a deep fusion of the Structural Information embodied in the concept sketch and the Semantic Information represented by the design prompts, resulting in a high-fidelity primary visual rendering.

3.3 Aerodynamic Performance Validation

Point Cloud Agent This Agent is responsible for generating the 3D Point Cloud from the rendering. In the context of our workflow, it takes the high-fidelity primary visual rendering as input and processes it to extract the necessary geometric information. This involves identifying key features and structures within the rendering, which are then mapped into a 3D space to create a detailed Point Cloud representation of the vehicle's body. We use 2 off-the-shelf models, a 3D diffusion model Zero-1to3 (Liu et al. 2023) and a 3D reconstruction model VGGT (Wang et al. 2025), to achieve this. The 3D diffusion model generates a set of standardized multi-view images from the rendering, as shown in Figure 5. While the 3D reconstruction model integrates and reconstructs them into a unified 3D point cloud capable of accurately representing the vehicle's body surfaces.



Figure 5: Multi-view images generated from the primary rendering.

Aerodynamic Prediction Agent With the 3D point cloud generated, the aerodynamic performance validation agent is responsible for predicting the aerodynamic characteristics of the vehicle design. Traditional CFD simulations are accurate but very slow, often taking hours or days for complex designs. To overcome this bottleneck, we employ a data-driven surrogate model in the agent whose core architecture is inspired by the Transolver (Wu et al. 2024). Transolver introduces a novel Physics-Attention mechanism, efficiently capturing intrinsic physical correlations from discretized geometries. Specifically, the Transolver architecture decomposes the discretized domain into learnable slices, assigning points with similar physical states to the same slice. These slices are encoded into physics-aware tokens, facilitating effective and computationally efficient attention-based predictions.

Physics Attention Calculation Given a set of point cloud $\mathbf{g} = \{\mathbf{g}_i\}_{i=1}^N$ with coordinate information of points N and observed quantities \mathbf{u} , a linear layer embeds them in deep features $\mathbf{x} = \{\mathbf{x}_i\}_{i=1}^N$, where each feature of the point cloud

contains C channels, i.e. $\mathbf{x}_i \in \mathbb{R}^{1 \times C}$, and involves both geometry and physics information. To capture physical states under the whole input domain, each point \mathbf{g}_i ascribed to M potential slices based on its learned feature \mathbf{x}_i , which is formalized as follows:

$$\{\mathbf{w}_i\}_{i=1}^N = \{\text{Softmax}(\text{Project}(\mathbf{x}_i))\}_{i=1}^N \quad (1)$$

$$\mathbf{s}_j = \{\mathbf{w}_{i,j} \mathbf{x}_i\}_{i=1}^N,$$

where $\text{Project}()$ projects the C channel feature into M weights and yields slice weights $\mathbf{w}_i \in \mathbb{R}^{1 \times M}$ after the $\text{Softmax}()$ operation. Specifically, $\mathbf{w}_{i,j}$ represents the degree to which the i -th point belongs to the j -th slice, with $\sum_{j=1}^M \mathbf{w}_{i,j} = 1$. $\mathbf{s}_j \in \mathbb{R}^{N \times C}$ denotes the j -th slice feature, which is a weighted combination of the N point features \mathbf{x} . Points with similar features will produce similar slice weights and are likely to be assigned to the same slice. To avoid uniform assignment across slices, $\text{Softmax}()$ are used along the slice dimension to encourage low-entropy and informative slice weight distributions.

Subsequently, since each slice aggregates points with similar geometric and physical characteristics, through spatially weighted aggregation encode them into physics-aware tokens.

$$\mathbf{z}_j = \frac{\sum_{i=1}^N \mathbf{s}_{j,i}}{\sum_{i=1}^N \mathbf{w}_{i,j}} = \frac{\sum_{i=1}^N \mathbf{w}_{i,j} \mathbf{x}_i}{\sum_{i=1}^N \mathbf{w}_{i,j}}, \quad (2)$$

where $\mathbf{z}_j \in \mathbb{R}^{1 \times C}$. Each token feature \mathbf{z}_j is normalized by dividing the sum of the corresponding slice weights. After encoding from physically consistent slices through spatial aggregation, each token captures the information of a specific physical state.

Formally, the physics attention mechanism among tokens is defined, for a deep feature $\mathbf{x} \in \mathbb{R}^{N \times C}$ embedded from input, firstly decompose it into M physically internal-consistent slices $\mathbf{s} = \{\mathbf{s}_j\}_{j=1}^M \in \mathbb{R}^{M \times (N \times C)}$ based on learned slice weights $\mathbf{w} \in \mathbb{R}^{N \times M}$. Then, to obtain the specific physics information contained in each slice, aggregate M slices to M physics-aware tokens $\mathbf{z} = \{\mathbf{z}_j\}_{j=1}^M \in \mathbb{R}^{M \times C}$ by Eq. (2). The attention mechanism among encoded tokens to capture intricate correlations among different physical states, that is

$$\mathbf{q}, \mathbf{k}, \mathbf{v} = \text{Linear}(\mathbf{z}), \quad \mathbf{z}' = \text{Softmax}\left(\frac{\mathbf{q}\mathbf{k}^T}{\sqrt{C}}\right) \mathbf{v}, \quad (3)$$

where $\mathbf{q}, \mathbf{k}, \mathbf{v}, \mathbf{z}' \in \mathbb{R}^{M \times C}$. Afterward, transited physical tokens $\mathbf{z}' = \{\mathbf{z}'_j\}_{j=1}^M$ are transformed back to mesh points by deslicing, which recomposes tokens with slice weights:

$$\mathbf{x}'_i = \sum_{j=1}^M \mathbf{w}_{i,j} \mathbf{z}'_j, \quad (4)$$

where $1 \leq i \leq N$ and each token \mathbf{z}'_j is broadcasted to all mesh points during above calculation.

Following the architecture of canonical Transformer, the l -th layer can be formalized as:

$$\hat{\mathbf{x}}^l = \text{Physics-Attn}(\text{LayerNorm}(\mathbf{x}^{l-1})) + \mathbf{x}^{l-1} \quad (5)$$

$$\mathbf{x}^l = \text{FeedForward}(\text{LayerNorm}(\hat{\mathbf{x}}^l)) + \hat{\mathbf{x}}^l,$$

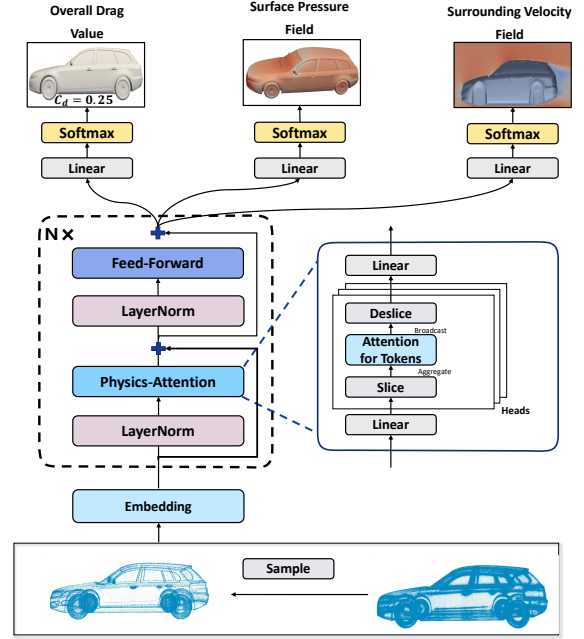


Figure 6: The model architecture. Sampled points are embedded and processed by L Transolver layers, then fed into three prediction heads for drag, pressure, and velocity field prediction.

where $l \in \{1, \dots, L\}$, $\mathbf{x}^l \in \mathbb{R}^{N \times C}$ is the output of the l -th layer, and $\mathbf{x}^0 \in \mathbb{R}^{N \times C}$ represents the input deep feature embedded from input geometries $\mathbf{g} \in \mathbb{R}^{N \times C_g}$ and initial observation $\mathbf{u} \in \mathbb{R}^{N \times C_u}$ via a embedding layer.

Model Architecture As shown in Figure 6, to address the computational challenges of large-scale 3D vehicle point clouds, we begin by applying a adaptive sampling strategy based on regional division of the raw input point cloud $\mathbf{g} \in \mathbb{R}^{N \times C_g}$ and its associated physical observations $\mathbf{u} \in \mathbb{R}^{N \times C_u}$. This strategy preserves key curvature features (upper part) and density-driven redundancy removal (lower part), effectively reducing the number of points while preserving essential geometric and physical information, enabling scalable inference.

The sampled points are then processed by an embedding layer that transforms the geometric coordinates and physical quantities into a unified deep feature representation $\mathbf{x}^0 \in \mathbb{R}^{N \times C}$. This embedding incorporates both spatial and physics-based context, forming the initial input to the main architecture.

The core of the model consists of a stack of L Transolver layers. Each layer integrates a Physics-Attention mechanism that dynamically slices and aggregates point features into physics-aware tokens. These tokens capture spatial and physical coherence across the domain and are refined through self-attention to learn complex inter-slice interactions. After attention-based token transformation, the information is projected back onto the point-wise representation via deslicing, enabling rich point-level feature updates. For-

	Aerodynamic Drag Prediction				
	MSE($\times 10^{-2}$) \downarrow	MAE($\times 10^{-1}$) \downarrow	R^2 Score \uparrow	Training Time (h)	Inference Time (s/sample)
TripNet	2.6020	4.0300	0.9720	-	-
PointNet	12.000	8.8500	0.8260	0.51	2.3
PointNet++	7.8130	6.7550	0.8960	0.52	2.4
GCNN	10.700	7.1700	0.8740	20.71	0.1
Ours	2.1044	4.4700	0.9740	1.75	2.1

	Surface Field Prediction				
	MSE($\times 10^{-2}$) \downarrow	MAE($\times 10^{-1}$) \downarrow	MAX AE \downarrow	Rel L_2 Error (%) \downarrow	Rel L_1 Error (%) \downarrow
TripNet	4.2300	1.1100	5.5200	20.3500	18.5200
FIGConvNet	4.3800	1.1300	5.7300	20.9800	18.5900
RegDGCNN	9.0100	1.5800	13.0900	28.4900	26.2900
Ours	3.9700	0.9600	7.9389	14.5600	9.7500

	Velocity Field Prediction				
	MSE \downarrow	MAE \downarrow	MAX AE \downarrow	Rel L_2 Error (%) \downarrow	Rel L_1 Error (%) \downarrow
U_x	6.52	1.06	31.12	9.77	7.42
U_y	2.16	0.92	24.09	32.93	27.42
U_z	2.10	0.97	25.88	33.43	31.45
U	6.27	1.85	29.32	6.63	10.78

Table 1: Performance comparison of our proposed model against several baseline methods for aerodynamic analysis. The evaluation covers three key prediction tasks: overall drag coefficient C_d , surface pressure field \mathbf{p} , and surrounding velocity field \mathbf{v} , assessed using various standard metrics.

mally, this process follows Eq. (5), iterating through L layers to obtain the final feature \mathbf{x}^L .

The resulting feature \mathbf{x}^L is then passed to three task-specific prediction heads, each implemented as a lightweight feed-forward decoder to predict the overall drag coefficient C_d , surface pressure field \mathbf{p} and surrounding velocity field \mathbf{v} .

This unified multi-task architecture enables the model to efficiently infer critical aerodynamic metrics in a single forward pass, substantially accelerating the design iteration cycle for aerodynamic performance evaluation.

Loss Function To simultaneously optimize for the three distinct outputs, the model is trained end-to-end using a composite loss function. For the high-dimensional field predictions, we follow the strategy outlined in the Shape-Net Car benchmark, which combines a loss for the surrounding velocity field (\mathcal{L}_v) and a loss for the surface pressure field (\mathcal{L}_p). Both are calculated using the Relative L2 error:

$$\mathcal{L}_{\text{field}} = \frac{\|\mathbf{y} - \hat{\mathbf{y}}\|_2}{\|\mathbf{y}\|_2}, \quad (6)$$

where \mathbf{y} is the ground-truth field and $\hat{\mathbf{y}}$ is the model’s prediction. For the scalar drag coefficient (C_d) prediction, we employ a standard MSE loss, denoted as \mathcal{L}_{C_d} . The total loss function, $\mathcal{L}_{\text{total}}$, is therefore defined as:

$$\mathcal{L}_{\text{total}} = \lambda_v \mathcal{L}_v + \lambda_s \mathcal{L}_p + \lambda_{C_d} \mathcal{L}_{C_d}, \quad (7)$$

By minimizing this composite loss, the model learns a balanced and unified feature representation capable of supporting all three prediction tasks.

4 Experiments

4.1 Experimental Setup

The core reasoning engine for each agent was powered by ”GPT-4o”. We trained and tested our Aerodynamic Prediction Agent on the DrivAerNet dataset (Elrefaie, Dai, and Ahmed 2025), which has 8,000 3D car models, each model comes with detailed CFD simulation data, including pressure, velocity, and drag coefficient. We implemented the model with $L = 6$ Transolver layers, an embedding dimension of $C = 256$, and $M = 64$ physics-aware slices. The model was trained for 200 epochs using the Adam optimizer with a learning rate of 0.001. The loss weights in Eq. 7 were set to $\lambda_v = 1.0$, $\lambda_p = 1.0$, and $\lambda_{C_d} = 0.1$.

4.2 Evaluation of Aerodynamic Prediction Performance

Main Result In Table 1, we present the results of three key prediction tasks: aerodynamic drag, surface field, and velocity field.

For aerodynamic drag prediction, our model is compared against methods including TripNet, PointNet, PointNet++, and GCNN. While TripNet achieves a slightly lower MAE, our model demonstrates highly competitive performance with a low MSE of 2.1044 and high R^2 score 0.9740, significantly outperforming PointNet and GCNN on this metric. At the same time, our model achieves a training time of 1.75 hours, which is significantly faster than GCNN’s 20.71 hours, while maintaining a near-instantaneous inference time of 2.1 seconds per sample compared with time-consuming CFD simulations.

In the surface field prediction task, our model shows superior performance by outperforming all listed baselines across key metrics. Notably, our model achieves the lowest Relative L_2 Error (14.56%) and Relative L_1 Error (9.75%), which indicates a more accurate prediction of the pressure distribution across the vehicle’s body compared to these other methods.

For the velocity field prediction, our model demonstrates strong performance across all three components of the velocity field (U_x , U_y , and U_z). The MSE values are 6.52, 2.16, and 2.10 respectively, with corresponding MAE values of 1.06, 0.92, and 0.97. The overall velocity field U achieves a MSE of 6.27 and an MAE of 1.85, indicating that our model effectively captures the complex fluid dynamics around the vehicle models.

Ablation Study We conducted an ablation study to investigate the impact of different sampling strategies and sample sizes on the performance of our surrogate model. We compared random sampling (*Rand*), curvature-based sampling (*Curvature*), and our proposed adaptive sampling strategy (*Adaptive*), evaluated at sample sizes of 10k, 20k, and 50k points. As shown in Table 2, Adaptive sampling outperforms both Curvature and Rand across all scales, with performance steadily improving as the sample size increases, demonstrating its efficiency and accuracy.

Sampling Method	MSE ↓	MAE ↓	R^2 ↑
Curvature-10k	1.9258	5.0010	0.8865
Curvature-20k	1.9075	4.9100	0.8848
Curvature-50k	1.8937	4.9006	0.8906
Adaptive-10k	1.8333	4.8410	0.8971
Adaptive-20k	1.7793	4.6105	0.8974
Adaptive-50k	1.7673	4.6007	0.9012
Rand-10k	1.9842	5.1070	0.8859
Rand-20k	1.8795	4.9440	0.8890
Rand-50k	1.8203	4.7284	0.8948

Table 2: Ablation study comparing different sampling methods and numbers of sampled points. Higher R^2 and lower MSE/MAE indicate better performance.

4.3 Evaluation of Conceptual and Creative Design

Human Evaluation As shown in Figure 7, to evaluate the quality of the generated concept sketches, we conducted a human evaluation study involving 10 professional automotive designers. Each participant reviewed a set of 100 concept sketches generated by our Rendering Generation Agent, and ranked them according to three criteria: creativity, aesthetic, and recognizability. Sketches produced by the Canny edge detection were used as a baseline. In addition, we conducted a second evaluation to assess the effectiveness of different input conditions in rendering generation. We tested three configurations: (1) sketches only, (2) design prompts only, (3) sketches + design prompts.

Objective Metrics Table 3 shows our quantitative evaluation results. CLIPasso sketches notably outperform the

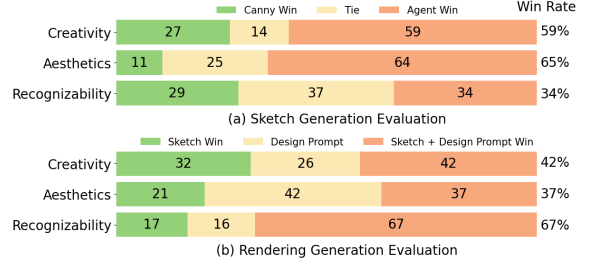


Figure 7: Human evaluation results for concept sketch generation and rendering quality across different input conditions.

Canny baseline in both FID and CLIP-Score. For renderings, combining sketches and prompts achieves the best semantic alignment and diversity.

Sketch Method	FID↓	CLIP-S↑	LPIPS↑
Canny Edge	47.11	26.04	0.54
Ours (CLIPasso)	40.02	29.40	0.58

Rendering Input	FID↓	CLIP-S↑	LPIPS↑
Sketch Only	35.7	28.13	0.44
Prompt Only	32.1	32.44	0.47
Sketch + Prompt	35.6	39.07	0.52

Table 3: Evaluation metrics of concept *sketches* and different input modalities on final *renderings*.

3D Reconstruction Result As shown in table 4, our pipeline achieves a 51% reduction in Chamfer Distance compared with Point-E and more than doubles the margin over the MCC baseline. Meanwhile, the IoU rises from 0.188 to 0.205. These gains confirm that leveraging multi-view diffusion priors before geometry fusion enables sharper edge recovery and fewer ghost points, which are crucial for downstream aerodynamic prediction.

	MCC	SJC-I	Point-E	Ours
CD ↓	0.0641	0.0571	0.0551	0.0265
IOU ↑	0.1386	0.1880	0.1880	0.2047

Table 4: Quantitative comparison of 3D reconstruction performance with respect to Chamfer Distance (CD) and Intersection-over-Union (IoU).

5 Conclusion

In this paper, we presented a novel two-stage multi-agent framework for automotive design, integrating conceptual design and aerodynamic performance validation. The framework orchestrate specialized agents, enabling rapid translation of user requirements into high-fidelity visual concepts and efficient aerodynamic analysis using a lightweight surrogate model. Our experimental results demonstrate the effectiveness of the proposed approach in automating the de-

sign process and achieving accurate aerodynamic predictions, significantly enhancing the efficiency of automotive design workflows.

References

- Alkin, B.; Bleeker, M.; Kurlle, R.; Kronlachner, T.; Sonnleitner, R.; Dorfer, M.; and Brandstetter, J. 2025. AB-UPT: Scaling Neural CFD Surrogates for High-Fidelity Automotive Aerodynamics Simulations via Anchored-Branched Universal Physics Transformers.
- Arechiga, N.; Permenter, F.; Song, B.; and Yuan, C. 2023. Drag-guided diffusion models for vehicle image generation.
- Burnap, A.; Hauser, J. R.; and Timoshenko, A. 2023. Product Aesthetic Design: A Machine Learning Augmentation. *Marketing Science*, 42(6): 1029–1056.
- Chen, G.; Yang, H.; Yu, B.; and Ren, H. 2025. Intelligent OPC Engineer Assistant for Semiconductor Manufacturing. *Proceedings of the AAAI Conference on Artificial Intelligence*, 39(22): 23144–23151.
- Chen, W.; Su, Y.; Zuo, J.; Yang, C.; Yuan, C.; Chan, C.; Yu, H.; Lu, Y.; Hung, Y.; Qian, C.; Qin, Y.; Cong, X.; Xie, R.; Liu, Z.; Sun, M.; and Zhou, J. 2024. AgentVerse: Facilitating Multi-Agent Collaboration and Exploring Emergent Behaviors. In *The Twelfth International Conference on Learning Representations, ICLR 2024, Vienna, Austria, May 7-11, 2024*. OpenReview.net.
- Elrefaie, M.; Dai, A.; and Ahmed, F. 2025. DrivAerNet: A Parametric Car Dataset for Data-Driven Aerodynamic Design and Prediction. *Journal of Mechanical Design*, 147(4).
- Elrefaie, M.; Qian, J.; Wu, R.; Chen, Q.; Dai, A.; and Ahmed, F. 2025. AI Agents in Engineering Design: A Multi-Agent Framework for Aesthetic and Aerodynamic Car Design.
- Goodfellow, I. J.; Pouget-Abadie, J.; Mirza, M.; Xu, B.; Warde-Farley, D.; Ozair, S.; Courville, A.; and Bengio, Y. 2014. Generative Adversarial Networks. arXiv:1406.2661.
- Gunpinar, E.; Coskun, U. C.; Ozsipahi, M.; and Gunpinar, S. 2019. A Generative Design and Drag Coefficient Prediction System for Sedan Car Side Silhouettes based on Computational Fluid Dynamics. *Computer-Aided Design*, 111: 65–79.
- He, J.; Luo, X.; and Wang, Y. 2025. DrivAer Transformer: A high-precision and fast prediction method for vehicle aerodynamic drag coefficient based on the DrivAerNet++ dataset.
- Ho, J.; Jain, A.; and Abbeel, P. 2020. Denoising Diffusion Probabilistic Models. In Larochelle, H.; Ranzato, M.; Hadsell, R.; Balcan, M.; and Lin, H., eds., *Advances in Neural Information Processing Systems 33: Annual Conference on Neural Information Processing Systems 2020, NeurIPS 2020, December 6-12, 2020, virtual*.
- Jacob, S. J.; Mrosek, M.; Othmer, C.; and Köstler, H. 2022. Deep Learning for Real-Time Aerodynamic Evaluations of Arbitrary Vehicle Shapes. *SAE International Journal of Passenger Vehicle Systems*, 15(2).
- Karras, T.; Laine, S.; and Aila, T. 2019. A Style-Based Generator Architecture for Generative Adversarial Networks. In *IEEE Conference on Computer Vision and Pattern Recognition, CVPR 2019, Long Beach, CA, USA, June 16-20, 2019*, 4401–4410. Computer Vision Foundation / IEEE.
- Kingma, D. P.; and Welling, M. 2014. Auto-Encoding Variational Bayes. In Bengio, Y.; and LeCun, Y., eds., *2nd International Conference on Learning Representations, ICLR 2014, Banff, AB, Canada, April 14-16, 2014, Conference Track Proceedings*.
- Labs, B. F.; Batifol, S.; Blattmann, A.; Boesel, F.; Consul, S.; Diagne, C.; Dockhorn, T.; English, J.; English, Z.; Esser, P.; Kulal, S.; Lacey, K.; Levi, Y.; Li, C.; Lorenz, D.; Müller, J.; Podell, D.; Rombach, R.; Saini, H.; Sauer, A.; and Smith, L. 2025. FLUX.1 Kontext: Flow Matching for In-Context Image Generation and Editing in Latent Space.
- Liu, J.; Li, H.; Chai, C.; Chen, K.; and Wang, D. 2025. A LLM-informed multi-agent AI system for drone-based visual inspection for infrastructure. *Advanced Engineering Informatics*, 68: 103643.
- Liu, R.; Wu, R.; Hoorick, B. V.; Tokmakov, P.; Zakharov, S.; and Vondrick, C. 2023. Zero-1-to-3: Zero-shot One Image to 3D Object. In *IEEE/CVF International Conference on Computer Vision, ICCV 2023, Paris, France, October 1-6, 2023*, 9264–9275. IEEE.
- Lu, J.; Pang, Z.; Xiao, M.; Zhu, Y.; Xia, R.; and Zhang, J. 2024. Merge, Ensemble, and Cooperate! A Survey on Collaborative Strategies in the Era of Large Language Models.
- Morita, H.; Shintani, K.; Yuan, C.; and Permenter, F. 2024. VehicleSDF: A 3D generative model for constrained engineering design via surrogate modeling.
- Qi, C. R.; Su, H.; Mo, K.; and Guibas, L. J. 2017. PointNet: Deep Learning on Point Sets for 3D Classification and Segmentation. In *2017 IEEE Conference on Computer Vision and Pattern Recognition, CVPR 2017, Honolulu, HI, USA, July 21-26, 2017*, 77–85. IEEE Computer Society.
- Qian, C.; Liu, W.; Liu, H.; Chen, N.; Dang, Y.; Li, J.; Yang, C.; Chen, W.; Su, Y.; Cong, X.; Xu, J.; Li, D.; Liu, Z.; and Sun, M. 2023. ChatDev: Communicative Agents for Software Development.
- Ramesh, A.; Pavlov, M.; Goh, G.; Gray, S.; Voss, C.; Radford, A.; Chen, M.; and Sutskever, I. 2021. Zero-Shot Text-to-Image Generation. In Meila, M.; and Zhang, T., eds., *Proceedings of the 38th International Conference on Machine Learning, ICML 2021, 18-24 July 2021, Virtual Event*, volume 139 of *Proceedings of Machine Learning Research*, 8821–8831. PMLR.
- Rombach, R.; Blattmann, A.; Lorenz, D.; Esser, P.; and Ommer, B. 2021. High-Resolution Image Synthesis with Latent Diffusion Models.
- Rosset, N.; Cordonnier, G.; Duvigneau, R.; and Bousseau, A. 2023. Interactive design of 2D car profiles with aerodynamic feedback. *Computer Graphics Forum*, 42(2): 427–437.
- SAHA, S.; RIOS, T.; MINKU, L.; STEIN, B.; WOLLSTADT, P.; YAO, X.; BACK, T.; SENDHOFF, B.; and

MENZEL, S. 2021. Exploiting Generative Models for Performance Predictions of 3D Car Designs. In *2021 IEEE Symposium Series on Computational Intelligence, SSCI 2021 - Proceedings*. United States: Institute of Electrical and Electronics Engineers Inc. ISBN 9781728190495. Publisher Copyright: © 2021 IEEE.

Schick, T.; Dwivedi-Yu, J.; Dessì, R.; Raileanu, R.; Lomeli, M.; Hambro, E.; Zettlemoyer, L.; Cancedda, N.; and Scialom, T. 2023. Toolformer: Language Models Can Teach Themselves to Use Tools. In Oh, A.; Naumann, T.; Globerson, A.; Saenko, K.; Hardt, M.; and Levine, S., eds., *Advances in Neural Information Processing Systems 36: Annual Conference on Neural Information Processing Systems 2023, NeurIPS 2023, New Orleans, LA, USA, December 10 - 16, 2023*.

Shinn, N.; Cassano, F.; Gopinath, A.; Narasimhan, K.; and Yao, S. 2023. Reflexion: language agents with verbal reinforcement learning. In Oh, A.; Naumann, T.; Globerson, A.; Saenko, K.; Hardt, M.; and Levine, S., eds., *Advances in Neural Information Processing Systems 36: Annual Conference on Neural Information Processing Systems 2023, NeurIPS 2023, New Orleans, LA, USA, December 10 - 16, 2023*.

Song, B.; Yuan, C.; Permenter, F.; Arechiga, N.; and Ahmed, F. 2023. Surrogate Modeling of Car Drag Coefficient with Depth and Normal Renderings.

Wang, J.; Chen, M.; Karaev, N.; Vedaldi, A.; Rupprecht, C.; and Novotny, D. 2025. VGGT: Visual Geometry Grounded Transformer. In *Proceedings of the IEEE/CVF Conference on Computer Vision and Pattern Recognition*.

Wu, H.; Luo, H.; Wang, H.; Wang, J.; and Long, M. 2024. Transolver: A Fast Transformer Solver for PDEs on General Geometries. In *Forty-first International Conference on Machine Learning, ICML 2024, Vienna, Austria, July 21-27, 2024*. OpenReview.net.

Wu, Q.; Bansal, G.; Zhang, J.; Wu, Y.; Li, B.; Zhu, E.; Jiang, L.; Zhang, X.; Zhang, S.; Liu, J.; Awadallah, A. H.; White, R. W.; Burger, D.; and Wang, C. 2023. AutoGen: Enabling Next-Gen LLM Applications via Multi-Agent Conversation.

Yao, S.; Zhao, J.; Yu, D.; Du, N.; Shafran, I.; Narasimhan, K. R.; and Cao, Y. 2023. ReAct: Synergizing Reasoning and Acting in Language Models. In *The Eleventh International Conference on Learning Representations, ICLR 2023, Kigali, Rwanda, May 1-5, 2023*. OpenReview.net.

Ye, Y.; Cong, X.; Tian, S.; Cao, J.; Wang, H.; Qin, Y.; Lu, Y.; Yu, H.; Wang, H.; Lin, Y.; Liu, Z.; and Sun, M. 2023. ProAgent: From Robotic Process Automation to Agentic Process Automation.

Zhang, L.; Fu, X.; Li, Y.; and Chen, J. 2025. Large language model-based agent Schema and library for automated building energy analysis and modeling. *Automation in Construction*, 176: 106244.

Zhang, L.; Rao, A.; and Agrawala, M. 2023. Adding Conditional Control to Text-to-Image Diffusion Models. In *IEEE/CVF International Conference on Computer Vision, ICCV 2023, Paris, France, October 1-6, 2023*, 3813–3824. IEEE.